Analysis of temporal and spatial variations in hydrometeorological elements in the Yarkant River Basin, China

Ren-juan Wei, Liang Peng, Chuan Liang, Christoph Haemmig, Matthias Huss, Zhen-xia Mu and Ying He

ABSTRACT

Yarkant River is a tributary of Tarim River in China, and the basin lacks observational data. To investigate past climatic variations and predict future climate changes, precipitation, air temperature and runoff data from Kaqun hydrological station are analysed at monthly and seasonal scales using detrended fluctuation analysis (DFA). Results show that DFA scaling exponents of monthly precipitation, air temperature and runoff are 0.535, 0.662 and 0.582, respectively. These three factors all show long-range correlations. Their increasing trends will continue in the near future as the climate shifts towards warmer and more humid. Spring and winter precipitation exhibit long-range correlations and will increase in the future. In contrast, summer and autumn precipitation exhibits random fluctuations and does not show stable trends. Air temperature during all seasons exhibits long-range correlations and will continue to increase in the future. Runoff during the spring and summer exhibits weak anti-persistence, but autumn and winter runoff show long-range correlations and increasing trends. The vertical distribution of precipitation was first analysed using observed data and climate reanalysis data. It indicates that precipitation increases with elevations below 2,000 m a.s.l. at a rate of 26 mm per 100 m and decreases with elevations above 2,000 m a.s.l.

Key words | air temperature, detrended fluctuation analysis, precipitation, runoff, spatial distribution, Yarkant River Basin

Ren-juan Wei
Chuan Liang
State Key Laboratory of Hydraulics and Mountain River Engineering,
College of Water Resource and Hydropower,
Sichuan University,
Chengdu 610065,
China

Ren-juan Wei
Sichuan Water Conservancy Vocational College,
Chengdu 611200,
China

Liang Peng (corresponding author)
Zhen-xia Mu
Ying He
College of Water Conservancy and Civil Engineering,
Xinjiang Agricultural University,
Xinjiang Urumqi 830052,
China
E-mail: *renjuan_wei@hotmail.com*

Christoph Haemmig
GEOTEST AG,
Zollikofen 3052,
Switzerland

Matthias Huss
Department of Geosciences,
University of Fribourg, Fribourg 1001,
Switzerland
and
Laboratory of Hydraulics,
Hydrology and Glaciology, ETH Zurich,
Zurich 8046,
Switzerland

INTRODUCTION

It is widely accepted that the global climate is changing, and the atmosphere is warming. Northern hemisphere air temperatures from 1983 to 2012 were higher than those over the past 1,400 years (IPCC 2013; Shen & Wang 2013). Furthermore, the hydrologic cycle is accelerating due to global warming. These changes can affect the water resource system, which is especially fragile in the arid areas of north-western China, where rivers are mainly fed by melt water from snow and ice (Chen *et al.* 2014). In this arid region, increases in precipitation have exceeded evaporation

doi: 10.2166/wcc.2018.111

due to the accelerated hydrologic cycle; therefore, the climate is trending towards warmer and wetter conditions (Arnell 1999; Shi *et al.* 2002). In southern Xinjiang, China, air temperature and precipitation have increased during the wet season. Simultaneously, climate warming has resulted in increases in snowline altitude and accelerated glacier melting (Gao *et al.* 2008).

The Yarkant River is located in north-western China (Figure 1). The river originates in the Karakoram Mountains, which are characterized by a dry climate with intense evaporation. Thus, changes in precipitation and air temperature will significantly influence runoff and may inhibit the management and utilization of water resources in Xinjiang. Several studies have focused on regional trends in water resources (Hao *et al.* 2008; Chen *et al.* 2014, 2017; Wang & Qin 2017). However, no comprehensive study has analysed recent hydrological trends or the distribution of precipitation in the Yarkant River Basin. Better understanding of the spatiotemporal trends in meteorological variables in the region will help improve projections of future water resources. The present study analyses trends in precipitation, air temperature and runoff.

As a key factor in the global water and energy cycles, spatially heterogeneous precipitation distributions can cause differences in plant populations among elevation zones. The vertical distribution of precipitation in alpine areas is influenced by many factors, including elevation, topography, slope, aspect and water vapour source. Several studies have examined the vertical distribution of precipitation. For example, the vertical distribution of precipitation in the western Tianshan Mountains was investigated using TRMM/TMI (Tropical Rainfall Measuring Mission/TRMM

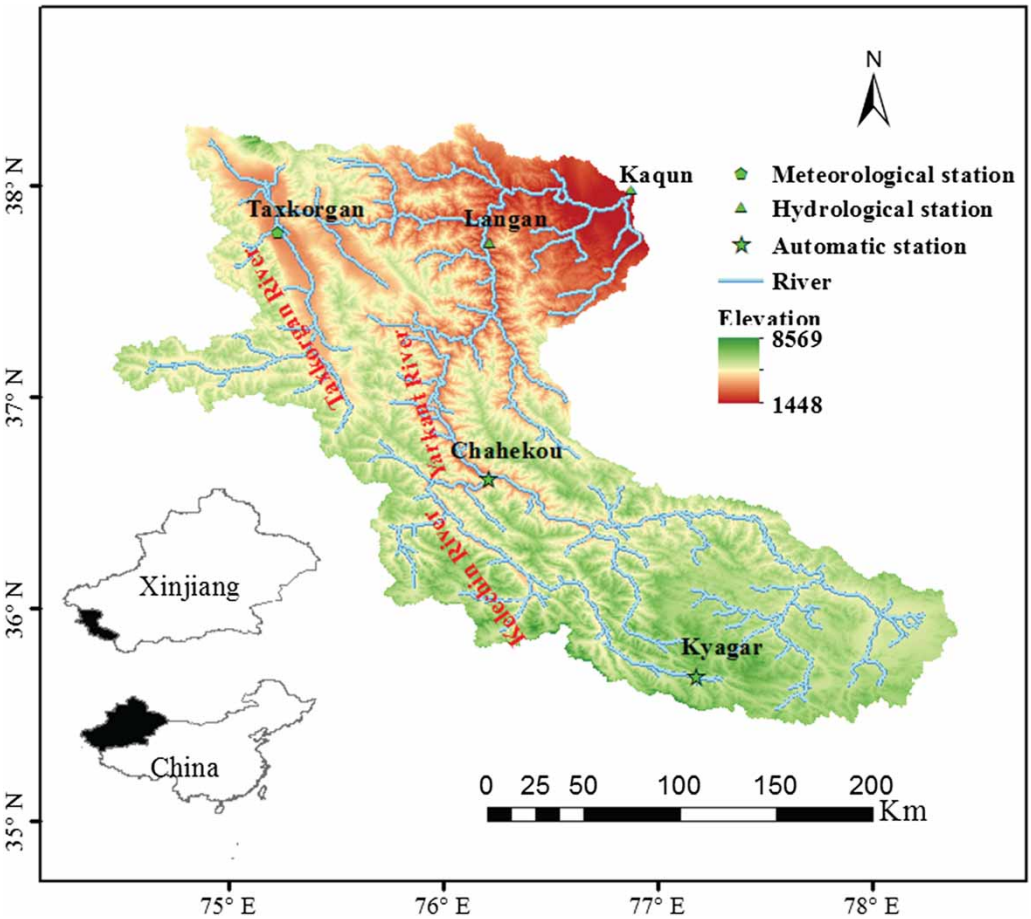

Figure 1 | The Yarkant River Basin and locations of hydrometeorological stations.

Microwave Imager) data, and the distribution was shown to be closely associated with topography (Mu & Jiang 2010). Additionally, the relationship between precipitation and elevation was investigated based on rainfall data from eight meteorological stations located at different elevations on the north-eastern and south-western slopes of the northern Ailao Mountains (Zhang *et al.* 1994). Conventional meteorological stations and hydrological stations in the Yarkant River Basin are rare, and most are located in low-altitude valley or plain areas; no stations are located in high-altitude alpine areas. In 2012, an international science and technology cooperation programme entitled 'Detecting and warning of glacier lake floods of the Yarkant River' (2012DFA20520) was carried out, sponsored by the Chinese Ministry of Water Resources. As part of the project, the following three automatic monitoring stations were established: Kyagar at 4,810 m a.s.l.; Chahekou at 2,990 m a.s.l.; and Langan at 1,920 m a.s.l. The detailed information on the three stations is shown in Figure 1 and Table 1. These stations produced daily hydrometeorological data from 2012 to 2015, providing a basis for investigating the vertical distribution of precipitation in the region (Haemmig *et al.* 2014; Peng *et al.* 2014). In recent decades, a number of precipitation products based on remote sensing data, interpolated station data, pattern matching results and other methods have improved hydrological studies in high alpine areas that are data-scarce (Getirana *et al.* 2011). The Climate Forecast System Reanalysis (CFSR) and China Meteorological Assimilation Driving Datasets for the SWAT model (CMADS) climate reanalysis products are two types of precipitation products that have been used in relevant studies.

The detrended fluctuation analysis (DFA) method was first introduced by Peng *et al.* (1994) in their study of correlations among the molecular chains of deoxyribonucleic acid. The method has the advantages of distinguishing intrinsic autocorrelation, eliminating local trends and false correlation phenomena, and accurately quantifying long-range correlations in non-stationary time series. DFA has been extensively used in studies of long-range correlation involving precipitation, air temperature, runoff, humidity and evaporation (Yue *et al.* 2010; Gao & Xu 2014; Wang *et al.* 2016).

In this study, monthly and seasonal precipitation, air temperature and runoff data from 1955 to 2015 from the Kaqun hydrological station (see Figure 1 and Table 1) in Xinjiang, China, are analysed using DFA to predict the future trends in these variables. Detailed information on the Kaqun hydrological station is shown in Figure 1 and Table 1. Additionally, the spatial distribution of precipitation in the Yarkant River Basin is analysed using observed data and the CMADS and CFSR reanalysis datasets. These datasets provide a scientific reference for further studies using hydrological models in the arid Yarkant Basin, which is expected to be affected by future climate change.

STUDY AREA AND MATERIALS

Study area

The Yarkant River originates from the Shenglidaban Glacier and the Kelechin River Valley on the northern slope of the Karakoram Mountains, Xinjiang, China. The basin (74°28′–80°54′E, 34°50′–40°31′N) is located on the southwestern margin of the Tarim Basin and is bordered by

Table 1 | Stations in the upper reach of the Yarkant River Basin

No.	Station	Type	Longitude (E)	Latitude (N)	Elevation (m)	Series length
1	Langan (1)	Hydrological station	76°12.2′	37°41.7′	2,000	1955–2015
2	Kaqun	Hydrological station	76°54.0′	37°59.0′	1,370	1955–2015
3	Taxkorgan	Meteorological station	75°15.8′	37°46.8′	3,090	1954–2013
4	Langan (2)	Automatic station	76°12.3′	37°41.2′	1,920	5/2013–6/2015
5	Chahekou	Automatic station	76°12.6′	36°36.6′	2,990	9/2012–6/2015
6	Kyagar	Automatic station	77°11.0′	35°40.6′	4,810	9/2012–6/2015

the ridge of the Karakoram Mountains and neighbouring Indus River Basin to the south. It is connected to the Hotan River Basin to the south-east and the Taklimakan Desert to the north-east. Additionally, the Yarkant River Basin is bordered by the Sarykol Range and Pakistan, Afghanistan and Tajikistan to the south-west and also neighbours the Basque and Aksu regions to the west and north (Wang 2010; Niu *et al.* 2011). The area of the basin is 5.02×10^4 km^2, and Kaqun hydrological station is located at the outlet. The terrain in the study region is rugged, with elevations ranging from 1,100 to 8,611 m a.s.l. The geographical positions and distribution of the hydrometeorological stations (Kan *et al.* 2013) are shown in Figure 1.

The Yarkant River Basin is far from the ocean, and its climate is mainly influenced by subpolar westerlies throughout the year and moderately influenced by the summer south-western monsoon from the Indian Ocean (Wang 2010). The basin contains almost 3,000 glaciers with an estimated ice volume of 660 km^3. The distribution of precipitation and temperature in the basin is extremely uneven. The average annual precipitation is approximately 30–60 mm. The mountain areas receive heavy precipitation, especially in the high-altitude region above 5,000 m a.s.l. The annual precipitation is approximately 150 mm in the middle and low-altitude areas (Gao *et al.* 2010). The annual average temperature near the average snowline in the glacier area is approximately −10.5°C (Ling *et al.* 2012). The Yarkant River Basin is a typical snow and ice-supplied river. Ice melt water and snowmelt are the main sources (accounting for approximately 64%) of runoff. Groundwater accounts for approximately 23% of the runoff in the basin, and precipitation accounts for approximately 13% (Fu *et al.* 2009). The distribution of runoff is extremely uneven throughout the year. According to data from Kaqun station, most runoff occurs from June to September, accounting for approximately 79.0% of the annual runoff. Runoff during the driest three months accounts for less than 5.9%. The average annual runoff is 66.14×10^8 m^3, with a coefficient of variation (Cv) of 0.17. The maximum annual runoff was 95.53×10^8 m^3 in 1994, and the minimum value was 44.68×10^8 m^3 in 1965. The ratio of the maximum to the minimum value is 2.14 (Wang *et al.* 2012). Based on the climate characteristics of the Yarkant River Basin, the seasons can be defined as follows: March to May is considered spring, June to August is summer, September to November is autumn, and December to February of the following year is winter.

Materials

Datasets from the Kaqun hydrological station in the Yarkant River spanning 1955 to 2015 were obtained from the Hydrological Almanac of Xinjiang and used for time series analysis. The data include total monthly precipitation, average air temperature and mean runoff. Observed meteorological data from Taxkorgan were downloaded from the website http://data.cma.cn and authorized for use by the China Meteorological Administration. Daily meteorological data from 2012 to 2015 collected by automatic monitoring stations (Langan (2), Chahekou and Kyagar; see Table 1) were obtained from a previous study of early warning systems for glacier lake floods in the Yarkant River Basin (Haemmig *et al.* 2014). The Shuttle Radar Topography Mission (SRTM3) digital elevation model (DEM) with a spatial resolution of 90 m was used to delineate the source region of the Yarkant River Basin. The CMADS dataset, which has a spatial resolution of $1/3^\circ \times 1/3^\circ$ and daily resolution from 2008 to 2014, was provided by the Cold and Arid Regions Science Data Centre at Lanzhou (http://westdc.westgis.ac.cn). The CFSR dataset from the National Centre for Environmental Prediction has a spatial resolution of $0.313^\circ \times 0.313^\circ$ and daily resolution covers the period from 1979 to 2014. The glacier dataset was provided by the Cold and Arid Regions Science Data Centre at Lanzhou (http://westdc.westgis.ac.cn). Detailed site information is provided in Table 1.

METHODS

Moving average method to remove seasonal cycles

The hydrological cycle is influenced by solar radiation. Periodic variations in radiation can cause seasonal changes in hydrometeorological elements, as well as variations in flow conditions and air temperatures. The moving average method was used to remove seasonal cycles and weaken periodic fluctuations in precipitation, air temperature and runoff data that could significantly influence the results of long-range correlation analyses.

For a time sequence $X(t) = (x_1, x_2, \ldots, x_n)$, the moving average ($MA$) can be calculated as follows (Qi 2012):

$$MA\left(t+\frac{N-1}{2}\right) = 1/N[x(t)+x(t+1)+\cdots+x(t+N-1)], \quad t = 1, 2, \cdots, n-N \tag{1}$$

where MA is the moving average, N is the period of fluctuations in the time sequence, and n is the total length of the time series. For a monthly series, N is equal to 12.

The centred moving average (CMA) is the average of MA and is calculated as follows:

$$CMA(t+N/2) = 1/2\left[MA\left(t+\frac{N-1}{2}\right)+MA\left(t+\frac{N+1}{2}\right)\right] \tag{2}$$

The ratio of $X(t)$ to the corresponding CMA is denoted as a scaling factor S, which can be calculated using the following expression:

$$S(t+N/2) = x(t+N/2)/CMA(t+N/2) \tag{3}$$

Average seasonal ratios were calculated for the spring, summer, autumn and winter; these ratios were defined as seasonal indices. A new time series can be obtained by removing the seasonal cycles; this series can be calculated by dividing the original series by a seasonal index.

DFA method

DFA, a method of calculating the scale exponent, was developed for long-range correlation analyses of non-stationary time series. The method can eliminate local trends and inherent variations in an original series that are reflected in the scale exponent. Briefly, DFA involves the following steps (Wang *et al.* 2016).

For a time sequence $X(t) = (x_1, x_2, \cdots, x_n)$, the cumulative deviation, denoted as $y(i)$, is computed by the following equation, where $\bar{x}$ is the mean of the original sequence and given by $\bar{x} = \sum_{t=1}^{n} x_t$, $(t = 1, 2, \cdots, n)$:

$$y(i) = \sum_{t=1}^{n} (x_t - \bar{x}), \ (i = 1, 2, \cdots, n) \tag{4}$$

In the next step, the cumulative deviation sequence is divided into non-overlapping boxes of equal length using the following equation:

$$Ns = \mathrm{int}(n/s) \tag{5}$$

Because n is not always an integral multiple of s, the sequence $y(i)$ is reversed and divided using the same method as above to ensure integrity of information. This process results in $2Ns$ boxes of equal length. A suitable value of s should be selected, and typical values of s range from $4 \leq s \leq \mathrm{int}(n/4)$.

The data in each box $v(v = 1, 2, \ldots, 2Ns)$ are fitted to $y_v(i)$ using a polynomial function of first, second, or a higher order, and each function represents the trend in a specific box. The integrated signal $y_s(i)$ is detrended by subtracting the local trend $y_v(i)$ in each box. The associated equation is as follows:

$$y_s(i) = y(i) - y_v(i), \ (i = 1, 2, \cdots, Ns) \tag{6}$$

The root-mean-square fluctuation is calculated as follows:

$$F^2(v, s) = \frac{1}{s}\sum_{i=1}^{s}\{y[(v-1)s+i] - y_v(i)\}^2, \ (i = 1, 2, \cdots, Ns) \tag{7}$$

$$F^2(v, s) = \frac{1}{s}\sum_{i=1}^{s}\{y[(N(v-N_s)s+i] - y_v(i)\}^2, \quad (i = Ns+1, Ns+2, \cdots, 2Ns) \tag{8}$$

The DFA fluctuation function of order q for a given sequence is calculated as follows:

$$F(s) = \sqrt[q]{\frac{1}{2Ns}\sum_{v=1}^{2Ns}\left[F^2(v, s)\right]^{\frac{q}{2}}} \tag{9}$$

A reliable power law relationship between $F(s)$ and s is determined, or a power law function is fitted using the least squares method, as follows:

$$F(s) \sim s^{\alpha} \tag{10}$$

$$\lg F(s) = \alpha \lg s + b \tag{11}$$

Fluctuations with respect to the local trend are characterized by the scaling index α. Five different cases can be distinguished: (1) there are no correlations (e.g., white noise), and the sequence is an independent random sequence for $\alpha = 0.5$; (2) the sequence is anti-persistent for $0 < \alpha < 0.5$, i.e., the data in the sequence are dependent; (3) the sequence has long-range correlation for $0.5 < \alpha < 1$; i.e., the data in the sequence are independent, they exhibit the same trend, and the closer the exponent α is to 1, the greater the sustained strength of the trend; (4) the sequence is a noisy sequence with a spectrum of 1/f for $\alpha = 1$; or (5) the sequence is a brown noise sequence for $\alpha \geq 1.5$.

RESULTS AND DISCUSSION

Temporal distribution of hydrometeorological elements

Removing seasonal cycles using the moving average method

The results in Figure 2 show the monthly runoff data from Kaqun station from 1955 to 2015 (a total of 732 values) with seasonal cycles removed using the MA method. The runoff time series exhibits smoother behaviour over time, that is, the cyclic seasonal fluctuations decrease. The same process was applied to the precipitation and air temperature datasets.

Analysis of cumulative deviation

The cumulative deviation of the time series reflects the cumulative fluctuations relative to the mean over time. If the cumulative deviation declines, the value of the time series is below the mean; otherwise, it is above the mean (Zhang 2010). The cumulative deviations for seasonal and annual precipitation, air temperature and runoff at Kaqun station from 1955 to 2015 were analysed, and the results are shown in Figure 3.

Different phases of variability exist for annual precipitation, annual average temperature and mean annual runoff at Kaqun station. (1) Precipitation shows a decreasing trend from 1955 to 1986, strong fluctuations between 1987 and 2002 and a notable increasing trend after 2002. (2) Variations in air temperature are more complex. The temperature significantly decreases from 1954 to 1962, fluctuates around the mean from 1963 to 1974, and decreases again from 1975 to 1978. From 1979 to 1990, no clear changes are apparent, and the temperature decreases again from 1990 to 1996. Overall, air temperature exhibits a decreasing trend from 1954 to 1996 and a substantial

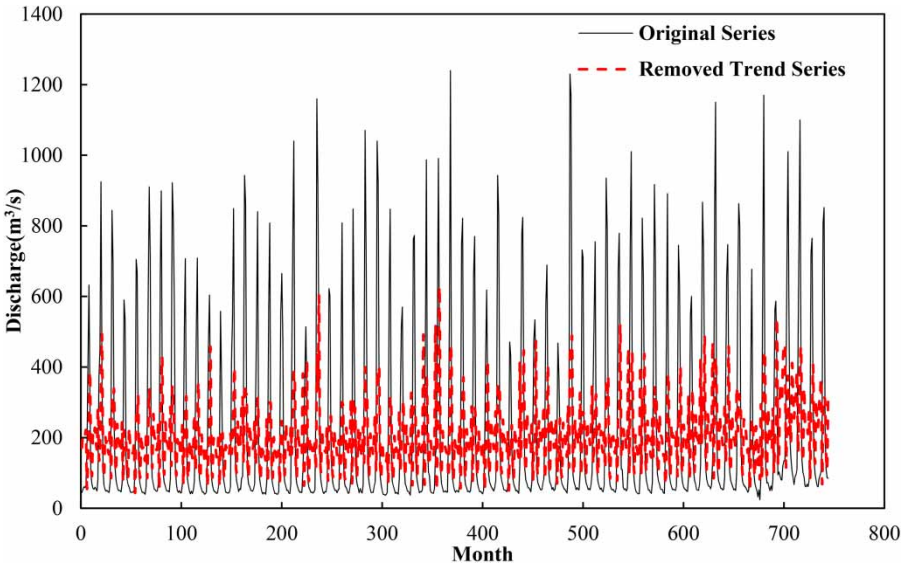

Figure 2 | Original runoff time series at Kaqun station and the series after local trend removal.

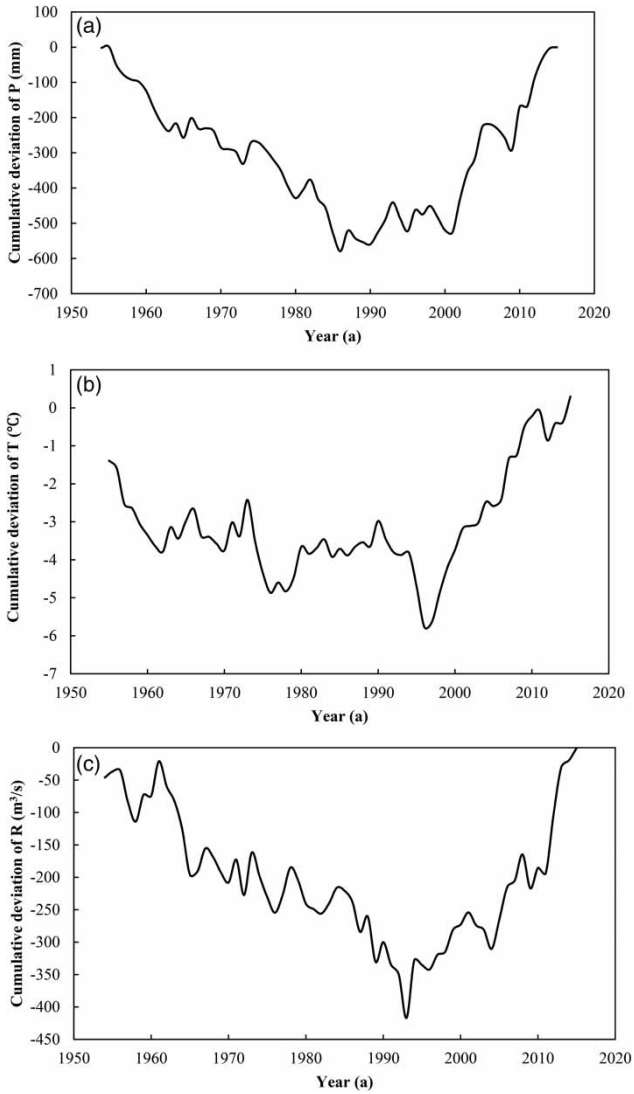

Figure 3 | Cumulative deviations in precipitation (a), air temperature (b) and runoff (c) based on monthly observations at Kaqun station. Annual precipitation, mean annual temperature and mean annual runoff are denoted by P, T and R, respectively, in Figure 3.

increasing trend after 1996. (3) For runoff, the cumulative deviation exhibits a decreasing trend from 1955 to 1993 and a clear increasing trend after 1993. Overall, precipitation, temperature and runoff increase from 1987, 1996 and 1993 to the present, respectively. After 1996, all the series display increasing trends. The increase in air temperature is consistent with climate warming, which also increases evapotranspiration. The amount of water vapour increases as evaporation increases, which leads to more precipitation. Moreover, increasing air temperature accelerates the melting of snow and ice, which contributes to enhanced runoff. Thus, these results indicate that the climate of the Yarkant River Basin has become increasingly warm and humid, which is consistent with the results of other studies (Shi *et al.* 2002; Chen *et al.* 2014).

DFA of monthly time series

Long-range correlations were calculated for monthly precipitation, temperature and runoff after removing the seasonal cycles. The fluctuation functions of the monthly time series are shown in Figure 4.

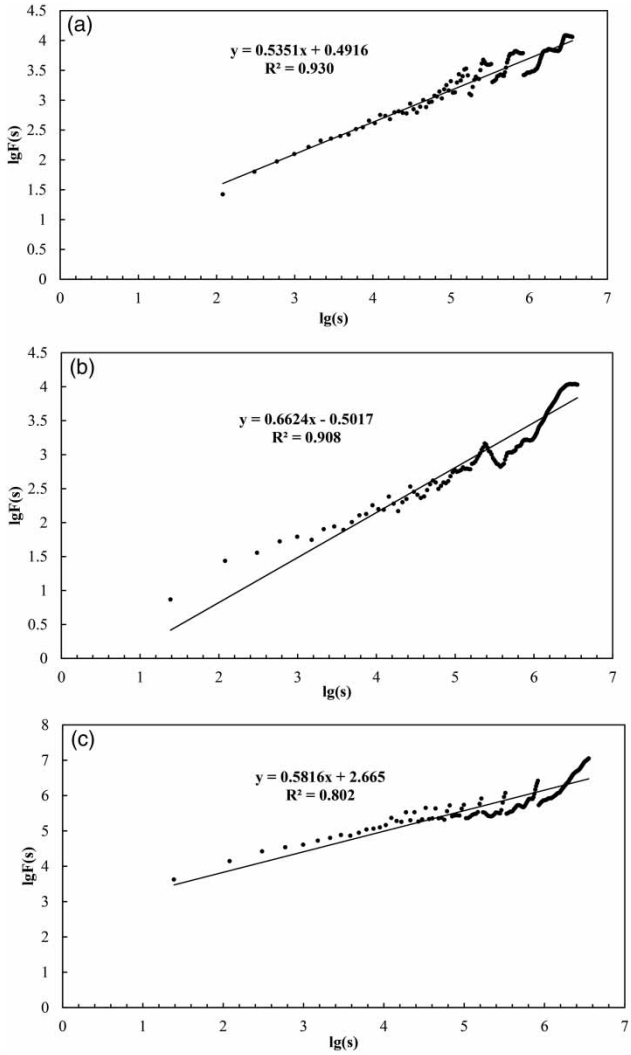

Figure 4 | Fluctuation functions of monthly precipitation (a), temperature (b) and runoff (c).

The results show linear correlation coefficients (R^2) between lgF(s) and lg(s) (see Equation (11)) of 0.930, 0.908 and 0.802 for precipitation, air temperature and runoff, respectively. All the correlations are significant. The DFA scaling exponents are 0.535, 0.662 and 0.582, which are all within the range of $0.5 < \alpha < 1$, indicating considerable long-range correlations. Therefore, all the variables (air temperature, precipitation and runoff) are likely to maintain the original trends in the near future, and the increasing trend in temperature contributes more to runoff than to precipitation. In combination with the cumulative deviation plots, these results suggest that precipitation, temperature and runoff will continue to increase in the future, with air temperature exhibiting the most notable change.

Analysis of seasonal cumulative deviations and DFA

Seasonal cumulative deviations in precipitation, temperature and runoff were analysed, and the results are shown in Figure 5. (1) Over the 61 years of investigation, there are no clear variations in the precipitation of winter, and the variance increases over time. During spring and autumn, precipitation changes are larger, with increasing trends after 2002 and 2000, respectively. Summer precipitation exhibits a decreasing trend from 1955 to 1986 and then increases greatly after 1987; this increase is the main cause of higher annual precipitation. (2) Air temperatures during the spring, autumn and winter all initially decrease and then increase, with change points in 1996, 1998 and 1978, respectively. Summer temperature is characterized by the opposite trend; it first increases and then decreases, with a change point in 1988. Thus, the summer temperature exhibits a trend opposite to that of the mean annual temperature. (3) Runoff during spring, summer, autumn and winter displays the same trend: first decreasing and then increasing. Spring runoff is stable from 1981 to 2004 and then increases. Summer runoff increases after 1992, following a period of stable fluctuations from 1968 to 1988.

The long-range correlations among the seasonal precipitation, temperature and runoff time series are analysed, and seasonal fluctuation functions are shown in Figure 6. There are differences among the fluctuation functions of seasonal precipitation. The scaling exponents of spring precipitation

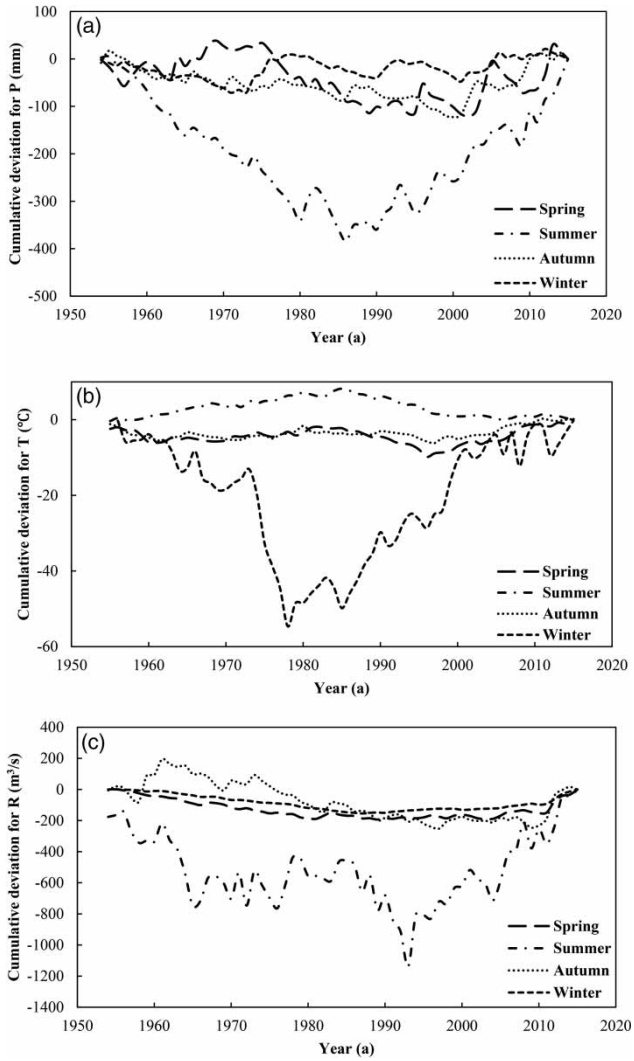

Figure 5 | Cumulative deviations in seasonal precipitation (a), temperature (b) and runoff (c) at Kaqun station.

and winter precipitation are 0.564 and 0.721, respectively. They both have long-range correlations, and the trends are expected to continue in the near future, with a greater trend in winter than in spring. Based on the analysis of the seasonal cumulative deviation, precipitation in spring and winter will increase in the near future. The scaling exponents in summer and autumn are 0.446 and 0.407, respectively, which are within the range of $0 < \alpha < 0.5$ and reflect white noise. Therefore, precipitation shows weak anti-persistence and strong randomness in these two seasons and is easily affected by local environment and external factors. The long-range correlations of spring and winter

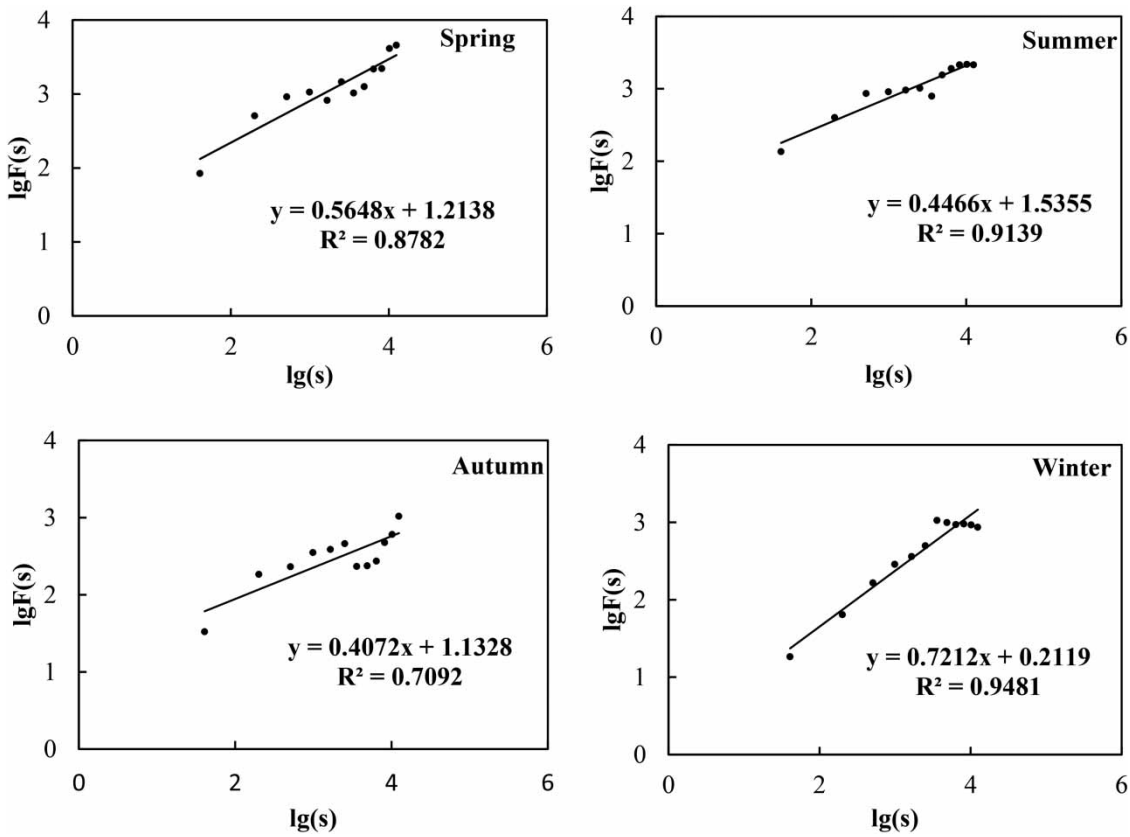

Figure 6 | Fluctuation functions in seasonal precipitation.

precipitation mainly contribute to correlations in the monthly precipitation time series.

The fluctuation functions of seasonal temperature (Figure 7) show that the long-range temperature correlations are consistent in all four seasons. The scaling exponents in spring, summer, autumn and winter are 0.821, 0.661, 0.646 and 0.729, respectively. All the exponents are in the range of $0.5 < \alpha < 1$ and reflect long-range correlations for air temperature in all four seasons. The same trends are sustained, with greater trends in spring and winter than in summer and autumn. In combination with the cumulative deviation plots for each season, temperatures in spring, autumn and winter are expected to increase, and the summer temperature is likely to continue decreasing. These results are consistent with those of previous studies (Liu & Wang 2009).

DFA was also conducted for seasonal runoff (results not shown). The scaling exponents of seasonal runoff are 0.415, 0.473, 0.530 and 0.557 for spring, summer, autumn and winter, respectively. The scaling exponents in spring and summer are in the range of $0 < \alpha < 0.5$, indicating weak anti-persistence and strong randomness in the two seasons, and easily affected by local environment and external factors. The scaling exponents in autumn and winter range from 0.5 to 1 and reflect long-range correlations. Therefore, the runoff in autumn and winter is expected to continue to increase.

Spatial analysis of precipitation in the Yarkant River Basin

Vertical distribution of observed precipitation

To investigate the accuracy and representativeness of the data from the Langan (2), Chahekou and Kyagar automatic monitoring stations, these data were compared with the data from three stations at similar elevations discussed in other references (Zheng & Zhang 1989; Zhang 1990; see Table 2).

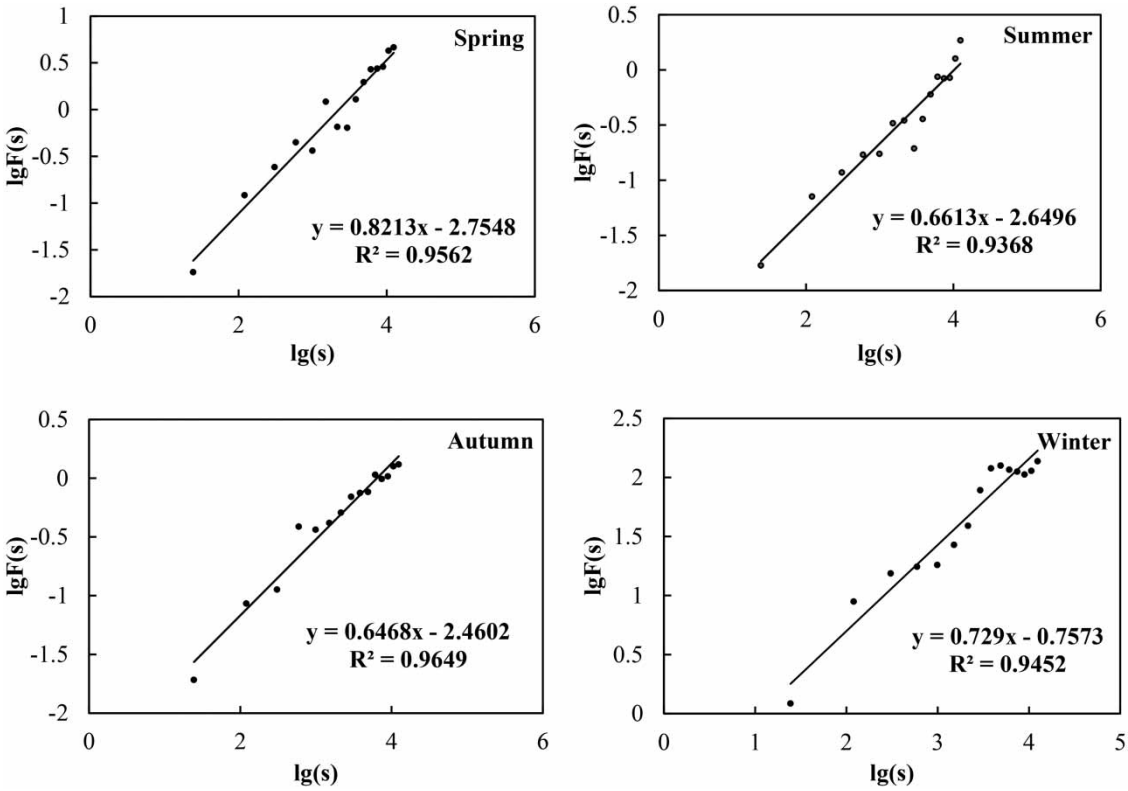

Figure 7 | Fluctuation functions in seasonal temperature.

Table 2 | Locations and average annual precipitation values of the observation stations

Station	Longitude (E)	Latitude (N)	Elevation (m)	Precipitation (mm)
Chahekou	76°12.6′	36°36.6′	2,990	62.9
Taxkorgan	75°15.8′	37°46.8′	3,091	72.0
Kyagar	77°11.0′	35°40.6′	4,810	8.87
Tianshuihai	79°36.0′	35°24.0′	4,900	23.8
Tianwendian	70°12.0′	35°18.0′	5,171	46.7
Kongkashankou	79°18.0′	34°42.0′	5,278	29.1

The elevation of the Chahekou automatic monitoring station is the same as that of the Taxkorgan observation station; the mean annual precipitation is 63 mm at Chahekou and close to 72 mm at Taxkorgan. The elevations of the Tianshuihai, Tianwendian and Kongkashankou stations are close to that of Kyagar station, and the annual precipitation values are 23.8, 46.7, 29.1 and 8.87 mm at these stations, respectively. The annual precipitation at Kyagar is low for different reasons, including the geographical location of the station. For example, Tianwendian station is located in the south-eastern Karakoram Mountains, which receive water vapour from the Indian Ocean that falls out in precipitation due to uplift along the mountain slopes. However, only small amounts of water vapour reach the highest parts of the northern Karakoram Mountains where Kyagar station is located (Figure 1).

The vertical distributions of annual and seasonal precipitation are analysed based on data from the same time period at all the stations from 2013 to 2014; the results are shown in Figure 8.

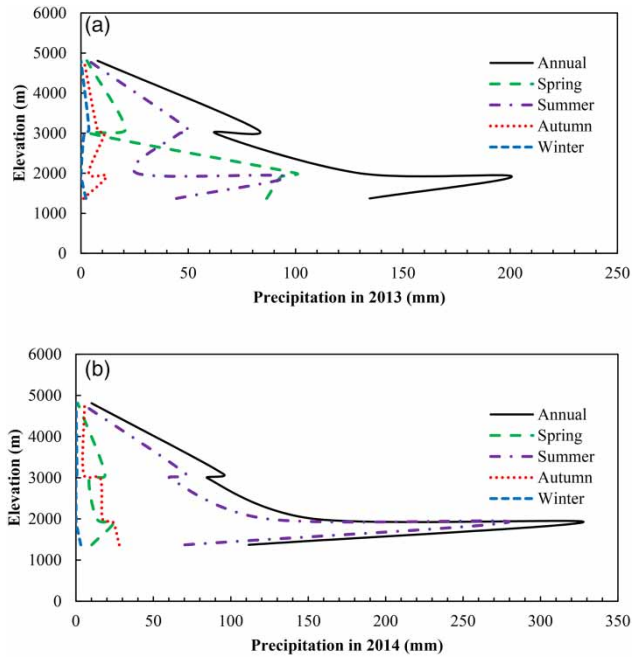

Figure 8 | Precipitation variations with elevation in 2013 (a) and 2014 (b).

The variations in precipitation with elevation in 2013 and 2014 exhibit a consistent pattern. Precipitation increases with elevation below 2,000 m a.s.l. and the precipitation gradient is 26 mm/100 m. Above 2,000 m a.s.l., precipitation gradually decreases, with a slight increasing trend at approximately 3,000 m. Next, precipitation significantly decreases. The mean annual value is only 8.87 mm at Kyagar station, which is consistent with the conclusion that precipitation is rare below the snowline in the Shaksgam Valley; this finding was deduced using hydrological methods of precipitation estimation in mountainous areas (Zhang 1991). The elevation and precipitation trends at the Taxkorgan and Chahekou stations are similar. A precipitation gradient of −4.6 mm/100 m is observed between Taxkorgan and Kyagar. Precipitation during the autumn and winter was rare in both 2013 and 2014. Precipitation in 2013 mainly occurred during the spring and summer; most precipitation occurred during the summer in 2014, with limited spring precipitation. The Karakoram Mountains are located in the southern and south-western portions of the Yarkant River Basin, whereas the northern and north-western portions of the basin are occupied by the Kunlun and Pamir Mountains. Glaciers are widely distributed in these mountains (Zhang 1991), and the existence of glaciers and their size depend on two conditions: low temperatures and large amounts of snow that exceed the amount of ablation in the upper parts of the glaciers. Of the two conditions, the amount of snow plays a dominant role. Thus, an increased amount of snow is assumed above the snowline.

Spatial distribution of precipitation based on CMADS and CFSR reanalysis data

The mean annual precipitation data from the CMADS and CFSR climate reanalysis products from 2008 to 2013 and observational data from reference stations were interpolated using kriging to determine the spatial variability in precipitation in the Yarkant River Basin. The results are shown in Figure 9.

The CMADS and CFSR data yield notably different precipitation distributions. The spatial variation characteristics of the CMADS data suggest higher precipitation in the east than in the west and a precipitation decrease from south to north, with a maximum in the south-east. However, the spatial distribution of CFSR data shows higher precipitation in the south-west than in the north-east and a maximum in the south-east. The spatially interpolated map of observed precipitation data shows that precipitation in the west is higher than in the east. The Yarkant River is far from the ocean and the climate of the area is controlled by westerlies. The south-western portion of the basin is influenced by water vapour from the Indian Ocean during summer (Wang 2010). Some studies have shown that the distribution of glaciers in the Karakoram Mountains is consistent with the precipitation distribution (Yang *et al.* 2012; Kan *et al.* 2013). Additionally, the precipitation distribution shown by the CFSR data is supported by the observed glacier distribution and is consistent with observed precipitation data. In contrast, the CMADS data underestimate precipitation in the south-western portion of the basin. The CMADS and CFSR data were extracted for the Kaqun, Langan, Taxkorgan, Chahekou and Kyagar stations and compared with the data collected at these stations. The results of this comparison are shown in Figure 10. The CMADS data are similar to the observed precipitation, though slightly higher; the CFSR values are substantially greater than the observed data, and the

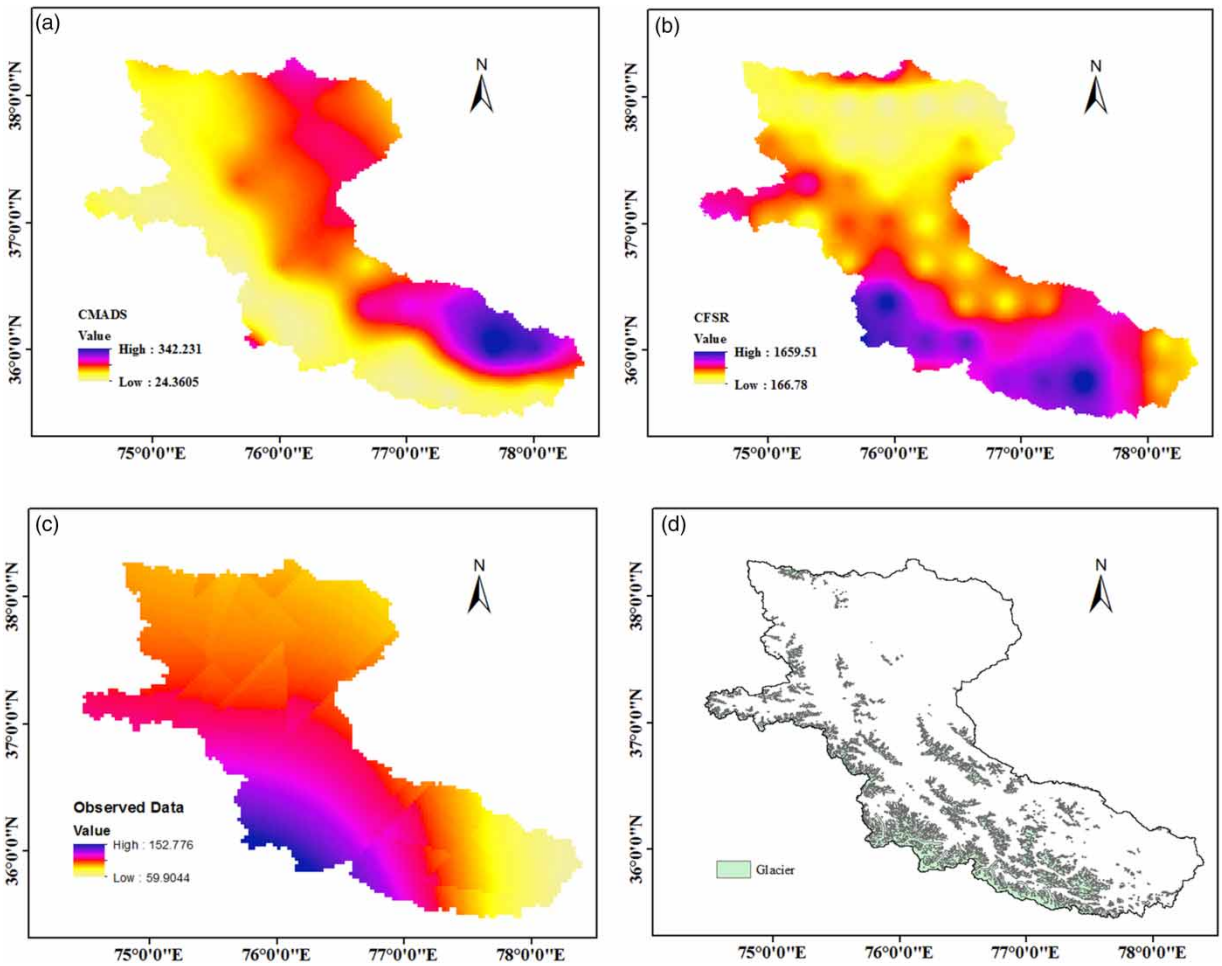

Figure 9 | Spatial distributions of precipitation and glaciers. The units of precipitation in (a), (b) and (c) are mm; the source of glacier data is the Cold and Arid Regions Science Data Centre at Lanzhou.

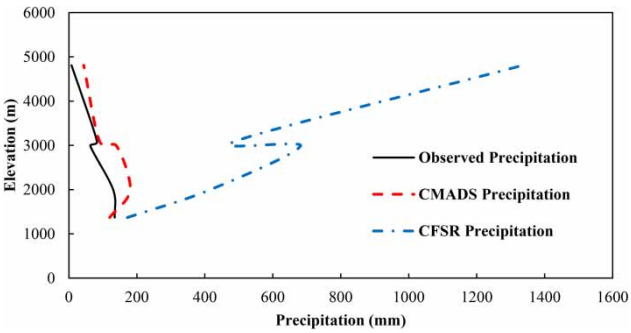

Figure 10 | Comparison of precipitation variations with elevation based on reanalysis data and observed data.

vertical precipitation gradients are not consistent with observations. Thus, while the CMADS data are suitable for the Yarkant River Basin, the spatial distribution of CMADS precipitation suggests that the product performs poorly in high-mountain glacier areas. Analyses of reanalysis data can provide the basis for further studies in high-alpine areas with no data, and modified CMADS data can be used in hydrological models to simulate runoff in the Yarkant River Basin.

CONCLUSIONS

DFA scaling exponents were calculated for the period from 1955 to 2015 based on monthly precipitation, air temperature and runoff at the Kaqun hydrological station; the values are 0.535, 0.662 and 0.581, respectively. The three variables all exhibited significant long-range correlations.

Thus, precipitation, temperature and runoff are expected to continue increasing in the future. The increasing trend is strongest for temperature, and the climate is becoming warmer and more humid.

The DFA scaling exponents for seasonal precipitation are 0.564 and 0.721 for spring and winter, respectively. Thus, precipitation during these seasons shows long-range correlations and is likely to continue increasing in the future. The scaling exponents in summer and autumn are 0.446 and 0.407, respectively. Therefore, precipitation shows weak anti-persistence and strong randomness in these two seasons and is easily affected by the local environment and by external factors. The DFA scaling exponents of air temperature in the four seasons are 0.821, 0.661, 0.646 and 0.729. All these values reflect long-range correlations, and the trends will likely be sustained in the near future. Spring, autumn and winter temperatures are expected to increase, and the summer temperature may decrease. The DFA scaling exponents of runoff are 0.415, 0.473, 0.530 and 0.557 for the four seasons, respectively. Runoff in spring and summer is weakly anti-persistent and shows strong randomness. Autumn and winter runoff shows long-range correlations and will continue increasing.

Direct observations indicate that precipitation increases at elevations below 2,000 m a.s.l. at a gradient of 26 mm per 100 m. Above 2,000 m a.s.l., precipitation gradually decreases. To sustain glaciers in the highest peaks of the Yarkant River Basin, there must be a considerable amount of snow in these areas. Therefore, despite the observed precipitation decreases between 2,000 and 5,000 m a.s.l., precipitation likely increases above the permanent snowline. The distribution of glaciers is consistent with the precipitation distribution. The distribution of precipitation shown by the CFSR reanalysis dataset is confirmed by the observed glacier distribution. Although the CMADS dataset underestimates precipitation in the south-western portion of the basin, it is more consistent with directly observed precipitation at monitoring stations than is the CFSR dataset. These climate reanalysis data can provide a basis for future studies of high alpine areas with no data; the CMADS data are more appropriate for use in hydrological models simulating runoff in the Yarkant River Basin.

ACKNOWLEDGEMENTS

The project is supported by the NSFC (51569031 and 51469034), ISTCP (2012DFA20520) and local authorities, including the Xinjiang Department of Water Resources, the Xinjiang Kashgar Hydrology Bureau and Kashgar Management Bureau of the Tarim River Basin. On the Swiss side, cooperation between the Swiss Agency for Development and Cooperation (SDC) and the Federal Office for the Environment (FOEN) supported the project.

REFERENCES

Arnell, N. W. 1999 Climate change and global water resources. *Global Environmental Change* **9**, 31–49.

Chen, Y. N., Li, Z., Fan, Y. T., Wang, H. J. & Fang, G. H. 2014 Research progress on the impact of climate change on water resources in the Arid Region of Northwest China. *Acta Geographica Sinica* **69** (9), 1296–1304. DOI:10.11821/dlxb201409005.

Chen, Q. Q., Chen, C. H. Q., Yang, Zh. Y. & Feng, J. 2017 Runoff variation in the Aksu River Basin and its response to climate change. *Journal of Water Resources & Water Engineering* **28** (1), 88–99. DOI:10.11705/j.issn.1672-643X.2017.01.15.

Fu, L. X., Chen, Y. N., Li, W. H., Xu, C. C. & He, B. 2009 Analyses of the durative and tendency of annual runoff in the headwaters of the Tarim River in the recent 50 years. *Journal of Glaciology and Geocryology* **31** (3), 457–463.

Gao, S. T. & Xu, C. C. 2014 Detrended fluctuation analyses on precipitation and air temperature in the headwaters of the Irtysh River basin over the last 50 years. *Journal of Glaciology and Geocryology* **36** (3), 707–716. DOI:10.7522/j.issn.1000-0240.2014.0085.

Gao, Q. Z., Wang, R. & Ernst, G. 2008 Impact of climate change on surface runoff of Tarim River originating from the south slopes of the Tianshan Mountains. *Journal of Glaciology and Geocryology* **30** (1), 1–11.

Gao, X., Zhang, S. Q., Ye, B. S. & Qiao, C. J. 2010 Glacier runoff change in the upper stream of Yarkant River and its impact on river runoff during 1961–2006. *Journal of Glaciology and Geocryology* **32** (3), 445–453. DOI:1000-0240(2010)03-0445-09.

Getirana, A. C. V., Espinoza, J. C. V., Ronchail, J. & Rotunno Filho, O. C. 2011 Assessment of different precipitation datasets and their impacts on the water balance of the Negro River basin. *Journal of Hydrology* **404**, 304–322. DOI:10.1016/j.jhydrol.2011.04.037.

Haemmig, C., Huss, M. & Keusen, H. 2014 Hazard assessment of glacial lake outburst floods from Kyagar glacier, Karakoram mountains, China. *Annals of Glaciology* **55**, 34–44.

Hao, X. M., Chen, Y. N., Xu, C. C. & Li, W. H. 2008 Impacts of climate change and human activities on the surface runoff in the Tarim River Basin over the last fifty years. *Water Resources Management* **22**, 1159–1171. DOI:10.1007/s11269-007-9218-4.

IPCC 2013 *Working Group I Contribution to the IPCC Fifth Assessment Report, Climate Change: The Physical Science Basis: Summary for Policymakers*. Cambridge University Press, Cambridge, UK and New York, USA.

Kan, B. Y., Su, F. G., Tong, K. & Zhang, L. L. 2013 Analysis of the applicability of four precipitation datasets in the upper reaches of the Yarkant River, the Karakorum. *Journal of Glaciology and Geocryology* **35** (3), 711–722. DOI:10.7522/j.issn.1000-0240.2013.0081.

Ling, H. B., Xu, H. L., Zhang, Q. Q., Liu, X. H., Fu, J. Y. & Bai, Y. 2012 Analysis on concentration and correlation of runoff and precipitation in the Yarkant River Basin. *Journal of Desert Research* **32** (6), 1758–1764. DOI: 1000-694X(2012)06-1757-08.

Liu, J. S. & Wang, D. 2009 A glacier surge found in the upstream area of Yarkant River, Karakorum Mountain, summer 2009. *Journal of Glaciology and Geocryology* **31** (5), 992.

Mu, Z. X. & Jiang, H. F. 2010 The vertical distribution law of precipitation in the Western Tianshan Mountain based on TRMM/TMI. *Journal of Arid Land Resources and Environment* **24** (10), 67–71.

Niu, J. F., Liu, J. S., Wang, D. & Kenneth, H. 2011 Monitoring on ice-dammed lake and related surging glaciers in Yarkant River, Karakorum in 2009. *Journal of Mountain Science* **29** (3), 277–282.

Peng, C. K., Buldyrev, S. V., Havlin, S., Simons, M., Stanley, H. E. & Goldberger, A. L. 1994 Mosaic organization of DNA nucleotides. *Physical Review E* **49** (2), 1685–1689.

Peng, L., Ao, Z. G., Chen, J. J. & Jiang, H. F. 2014 Design and application of monitoring and early warning to Kyagar glacier lake in the Karakorum mountain. *Journal of Water Resources & Water Engineering* **25** (5), 124–131. DOI:10.11705/j.issn.1672-643X.2014.05.027.

Qi, X. W. 2012 *Study of Characteristics of Runoff Time Series Based on Fractal Theory*. Master's thesis, Huazhong University of Science and Technology, Wu Han, China.

Shen, Y. P. & Wang, G. Y. 2013 Key findings and assessment results of IPCC WGI Fifth Assessment Report. *Journal of Glaciology and Geocryology* **35** (5), 1068–1076. DOI:10.7522/j.issn.1000-0240.2013.0120.

Shi, Y. F., Shen, Y. P. & Hu, R. J. 2002 Preliminary study on signal, impact and foreground of climatic shift from warm-dry to warm-humid in Northwest China. *Journal of Glaciology and Geocryology* **24** (3), 220–226.

Wang, S. J. 2010 *The Rivers in Xinjiang of China*. China Water Power Press, Beijing, China.

Wang, Y. J. & Qin, D. H. 2017 Influence of climate change and human activity on water resources in Arid Region of Northwest China: an overview. *Climate Change Research* **13** (5), 483–493. DOI:10.12006/j.issn.1673-1719.2017.004.

Wang, X. N., Huang, Q. & Chang, J. X. 2012 Analysis on the law of runoff in the Yarkant River of Xinjiang. *Yellow River* **34** (6), 45–50.

Wang, Z., Liang, C., Zhao, P. & Zhan, C. 2016 Long-range correlation of surface dry/wet condition and its influential factors in hilly area of central Sichuan. *Journal of Sichuan University (Engineering Science Edition)* **48** (1), 62–68. DOI:10.15961/j.jsuese.2016.s1.010.

Yang, X. G., Qin, D. H. & Qin, X. 2012 Progress in the study of interaction between ice/snow and atmosphere. *Journal of Glaciology and Geocryology* **34** (2), 393–402.

Yue, J. H., Zhao, X. J. & Shang, P. J. 2010 Effect of trends on detrended fluctuation analysis of Precipitation Series. *Mathematical Problems in Engineering* **2010**, 1–15. DOI:10.1155/2010/749894.

Zhang, B. P. 1990 Physical features and vertical zones of the Karakoram and Ali-Karakoram Mountains. *Journal of Arid Land Resources and Environment* **4** (2), 49–63.

Zhang, X. S. 1991 *Glacier and Environment of Yarkant River in Karakoram*. Science Press, Beijing, China.

Zhang, R. R. 2010 Trend and evolution of precipitation in Hong Kong. *Journal of Hohai University (Natural Sciences)* **38** (5), 505–510. DOI:10.3876/j.issn.1000-1980.2010.05.005.

Zhang, K. Y., Zhang, Y. P., Liu, Y. H. & Li, Y. R. 1994 Vertical distribution characteristics of rainfall in the Ailao Mountain. *Scientia Geographical Sinica* **14** (2), 144–151. DOI:10.13249/j.cnki.sgs.1994.02.006.

Zheng, D. & Zhang, B. P. 1989 A study on the altitudinal belts and environmental problems of the Karakoram and West Kunlun Mountains. *Journal of Natural Resources* **4** (3), 255–266.

First received 9 April 2017; accepted in revised form 3 April 2018. Available online 7 May 2018